



UNIVERSITY OF LEEDS

This is a repository copy of *Experimental study on dielectric relaxation of SiO<sub>2</sub> nano-particle suspensions for developing a particle characterization method based on electrical impedance spectroscopy*.

White Rose Research Online URL for this paper:  
<http://eprints.whiterose.ac.uk/88896/>

Version: Accepted Version

---

**Article:**

Zhao, Y and Wang, M (2015) Experimental study on dielectric relaxation of SiO<sub>2</sub> nano-particle suspensions for developing a particle characterization method based on electrical impedance spectroscopy. *Powder Technology*, 281. 200 - 213. ISSN 0032-5910

<https://doi.org/10.1016/j.powtec.2015.04.070>

---

© 2015 Elsevier. Licensed under the Creative Commons Attribution-NonCommercial-NoDerivatives 4.0 International  
<http://creativecommons.org/licenses/by-nc-nd/4.0/>

**Reuse**

Unless indicated otherwise, fulltext items are protected by copyright with all rights reserved. The copyright exception in section 29 of the Copyright, Designs and Patents Act 1988 allows the making of a single copy solely for the purpose of non-commercial research or private study within the limits of fair dealing. The publisher or other rights-holder may allow further reproduction and re-use of this version - refer to the White Rose Research Online record for this item. Where records identify the publisher as the copyright holder, users can verify any specific terms of use on the publisher's website.

**Takedown**

If you consider content in White Rose Research Online to be in breach of UK law, please notify us by emailing [eprints@whiterose.ac.uk](mailto:eprints@whiterose.ac.uk) including the URL of the record and the reason for the withdrawal request.



[eprints@whiterose.ac.uk](mailto:eprints@whiterose.ac.uk)  
<https://eprints.whiterose.ac.uk/>

**Experimental Study on Dielectric Relaxation of SiO<sub>2</sub>  
Nano-particle Suspensions for Developing a Particle  
Characterization Method based on Electrical Impedance  
Spectroscopy**

Yanlin Zhao<sup>1\*</sup> and Mi Wang<sup>2</sup>

<sup>1</sup>Department of Thermal Energy Engineering, College of Mechanical and  
Transportation Engineering, China University of Petroleum, Beijing 102249, People's  
Republic of China (Tel: +86-10-89733658, Email: ylzhao1212@hotmail.com)

<sup>2</sup>Institute of Particle Science & Engineering, School of Chemical and Process  
Engineering, University of Leeds, Leeds LS2 9JT, United Kingdom (Tel: +44 (0) 113  
343 2435, Email: m.wang@leeds.ac.uk)

\*Corresponding author

## Abstract

In this paper, the dielectric relaxation of SiO<sub>2</sub> nano-particle suspensions is studied by electrical impedance spectroscopy method. The case of suspension composed of particles with thick double layer is concerned. The objective of this study is to find out the relationship between particle properties (size and concentration) and electrical impedance spectroscopy for developing a particle characterization method based on electrical impedance spectroscopy/tomography. The influences of particle size on electrical impedance spectroscopy (EIS) and relaxation frequency are investigated and analyzed. The experimental results indicate that impedance phase angle and  $\alpha$  relaxation frequency are functions of particle size.  $\alpha$  relaxation frequency is proportionally changing with  $(a + \kappa^{-1})^{-n}$  ( $a$  is particle radius,  $\kappa^{-1}$  is double layer thickness,  $n$  equals 0.344 for 4.76% suspension and 0.308 for 2.38% suspension). The exponent term,  $n$ , is smaller than the one in dilute suspensions ( $n=2$ ), which is possibly due to decreasing of diffusion distance of ions around the particles in concentrated suspensions with thick double layer. The impedance parameters, including conductivity increment,  $\Delta K'$ , and  $\alpha$  relaxation frequency are influenced by particle volume fraction. The conductivity increment,  $\Delta K'$  becomes less negative with increasing particle volume fraction due to the positive contribution of double layer charge on the conductivity increment. The  $\alpha$  relaxation frequency increases with increasing particle volume fraction and the small particles show a more significant increase than large particles. The experimental result on the differential electrical impedance tomographic images between the silica suspension and water (with same

conductivity value) shows that small differences on the values of impedance imaginary part and phase can be observed at the upper right corner in the EIT images, which represent a small differentiation on the dielectric property caused by the electrical polarization of double layer on the particle surface.

**Keywords:** Electrical impedance spectroscopy, dielectric relaxation, electrical double layer, relaxation frequency, tomographic image

## 1. Introduction

Electrical impedance spectroscopy (EIS) is a powerful technique to characterize the electrokinetic properties of materials and particle-solution interfaces[1,2]. The nano-particles in aqueous suspensions usually carry surface charge and have an electrical double layer at the particle-solution interface. In EIS measurement, the charged particles and its double layer could be driven to motion by an applied alternating electric field, with the particle and counterions at the surface moving in opposite direction[3]. As a result, the polarization of electrical double layer can be formed and measured by electrical impedance spectra. The complex impedance, conductivity, and permittivity are highly sensitive to the characteristics of particles and disperse medium, including double layer thickness, surface charge, particle size, particle volume fraction, and the associated zeta potential etc.[4-5]. Hence, the development of electrical impedance spectroscopy method provides a possibility for

characterizing the nano-particles (particle size and particle concentration) in aqueous suspension relying on the polarization of charged particles and double layer.

With increasing requirements for on-line controlling/monitoring of process variables in many industrial processes (e.g. crystallization), the study and development of on-line method for characterizing particles in aqueous suspensions has become more valuable[6-8]. The current commercially available methods mainly rely on optical techniques, such as laser diffraction[9], focused beam reflectance measurement (FBRM)[10-11], and multiple light scattering[12], and digital video microscope[13]. Except for the FBRM technique, other optical techniques are inherently suitable for examining the diluted suspensions and require sample dilution before measurement. The FBRM technique is not accurate for the non-spherical particles and can only get the distribution of chord length, not the true particle size due to its measurement principle[14]. The non-optical techniques, such as ultrasonic attenuation spectroscopy and synchrotron X-ray diffraction, are relatively complex, expensive and involve safety problem, thus they are not widely used in industries. In addition, the requirement of visualization of control parameters in a process control system need to monitor not only the particle size/concentration, but also the images of particle size/concentration distribution, even the spatial distribution of particle size/concentration under different operation conditions. Therefore, the current state of on-line characterizing methods of nano-particles in suspensions shows an attractive prospect for development of new techniques and encourages further development in both experimental and theoretical aspects.

Electrical impedance tomography (EIT) is one of the process tomography techniques to provide an on-line non-invasive imaging measurement on concentration profiles and characterization of the fluid dynamics in industrial applications[15-18]. In EIT measurement, the voltage is measured from a number of paired electrodes of tomography sensor and the distribution of the conductivity or other impedance parameters can be obtained by a process of data reconstruction. There are two types of algorithms for data reconstruction, qualitative algorithms and quantitative algorithms. The qualitative algorithm depicts a change in voltage relative to initially acquired reference data. It utilizes a back projection algorithm, as a typical example, which can be performed by multiplying a pre-calculated sensitivity map (matrix) to a relative voltage change (vector) to reconstruct images[19]. This algorithm is simple and fast but not accurate enough. For accurately reconstructing images, a quantitative algorithm is required, which utilizes multistep iterative method to solve the inverse problem of a nonlinear electric field. As one of the quantitative algorithm, sensitivity theorem based inverse solution using conjugate gradient method (acronym SCG) could greatly reduce the effects of electrode modeling errors, decrease the instrumental errors, subtract the background and highlight the low contrast change in the region of interest[20]. Therefore, SCG method could provide a possibility to obtain the differential images when the impedance difference between the continuous phase and disperse phase is very small. Details of the SCG algorithm can be found elsewhere[20]. The measurement strategy of EIS is basically same to that of electrical impedance tomography (EIT) as the excitation is applied to a pair of electrode and the

response is measured by another pair of electrode. It is known that the current applications of EIT in the process industries rely on the conductivity difference caused by the particles in the suspensions. The data of impedance imaginary part and phase angle have not been utilized to reveal the characterization of particles (size or concentration). Based on the same measurement strategy, the study of EIS method on characterizing nano-particles could provide the fundamental knowledge for developing the electrical impedance tomography (EIT) technique on characterizing the spatial distribution of particle properties.

The polarization of charged particles and double layer under alternating electric field has been studied by the dielectric relaxation of nano-particle suspensions[21-26]. The effect of particle size and concentration on dielectric properties has been studied using the permittivity spectroscopy[27-31]. The relationship between the particle size and electrical impedance spectra during crystallization process of L-glutamic acid has been studied by Zhao *et al.*[32]. The early researches started from the relatively simple systems with thin double layer and dilute suspensions. More complicated systems, for example, thick or arbitrary double layer thickness and concentrated suspensions were studied afterwards. However, many researchers carried out the theoretical studies relying on the numerical simulation [33-35]. A numerical study which discussed the effect of size polydispersity of colloidal suspensions on their dielectric properties was carried out by Carrique *et al.*, [33]. The simulation results show that there is no difference in the dielectric increments obtained from a monodisperse suspension and a polydisperse suspension which have the same

volume-averaged mean radius. Arroyo *et al.* [34] compared the particle size effect in the dielectric increment of colloidal suspensions using two theoretical models, Delacey and White model (DW) and DW model including a dynamic stern layer (DSL). The results show that at the low-frequency, difference between two models is negligible for small particles, but becomes significant with increasing particle size. Carrique *et al.* [35] studied the dielectric response of a concentrated colloidal suspension in a salt-free medium by simulation. The results show that both  $\alpha$  and MWO relaxation frequencies move to the high frequency side with decreasing particle size under the conditions of fixed volume fraction and particle charge density. The experimental studies focusing on the particle size and concentration effects on dielectric relaxation of nano-particle suspensions are still very limited, especially in the suspensions with thick double layer and various particle volume fractions. Therefore, in this paper, the dielectric relaxation of SiO<sub>2</sub> nano-particle suspensions was studied experimentally using electrical impedance spectroscopy. The influences of particle size and particle volume fraction on dielectric properties of silica nano-particle suspensions were investigated by electrical impedance spectroscopy and permittivity spectra. Finally, the responses of electrical polarisation of silica particles on electrical impedance tomographic images are studied.

## **2. Experiment details**

### *2.1. Experiment setup for EIS measurement*

Experiments on colloidal suspensions were carried out using a vessel with a four-electrode sensor (Figure 1). The four-electrode sensor includes two plate electrodes and two needle electrodes, which are all made of stainless steel. The two plate electrodes are designed in a square shape with dimensions of 40 mm×40 mm, and the distance between two electrodes is 30 mm. Two needle electrodes are put in the middle of the two plate electrodes. The diameter of the needle is 0.337 mm and the distance between the two needle electrodes is 10 mm. Comparing the distance between the two plate electrodes and the size of needle electrodes, the two plate electrodes are much bigger in surface area, therefore it can be assumed that the electric field is parallel and uniform between the two plates and the interference of the two needle electrodes to the field can be ignored in the model. In experiments, the vessel was filled with colloidal sample. The EIS measurement was carried out by applying an alternating excitation voltage (1 volt) with a frequency spectrum from 1 Hz to 32 MHz to the two plate-electrodes and taking the EIS response from the two needle electrodes. The electrical impedance spectra were obtained using a Solartron 1260 Impedance/Gain-Phase Analyzer that controlled, with the SMaRT software.

## *2.2. Experiment setup for EIT measurement*

The devices for electrical impedance tomography (EIT) measurement include a cylinder shaped vessel with a 16-electrode sensor, a Perspex chamber and the Z8000 instrument (ITS). The Perspex chamber is a hollow square with a hole on top for adding the testing silica suspension. The dimensions of the Perspex chamber are a height of 125 mm, length of 20 mm, width of 62 mm and the aperture on top is 10 mm

in diameter. The dimensions of the chamber and ERT vessel are shown in Table 1. Cling film was glued on both sides of the chamber to hold the silica suspension to prevent leakage. In order to measure tomography imaging of silica suspension (water as reference), a chamber was put into the cylindrical vessel and fixed by clamps. Figure 2 shows photograph of a Perspex chamber fixed in a cylindrical vessel. The EIT measurement was carried out using silica suspension (220nm silica original sample with concentration of 23.5wt% and conductivity of 1.1ms/cm) and distilled water whose conductivity value was adjusted to 1.1ms/cm using 1M KCl. The purpose using same conductivity water as reference is to minimize the effect from different conductivity. Totally four experiments were carried out by using different reference and the details are shown below:

(1) The empty chamber was fixed in the vessel, which is filled by water ( $\sigma = 1.1 \text{ ms/cm}$ ).

The reference is water.

(2) The chamber was filled by water ( $\sigma = 1.1 \text{ ms/cm}$ ) and then fixed in the vessel, which is also filled with water ( $\sigma = 1.1 \text{ ms/cm}$ ) as well. The reference is empty chamber + water ( $\sigma = 1.1 \text{ ms/cm}$ ) in vessel.

(3) The chamber was filled by silica suspension (220 nm, 23wt%,  $\sigma = 1.1 \text{ ms/cm}$ ) and then fixed in the vessel, which is filled by water ( $\sigma = 1.1 \text{ ms/cm}$ ) as well. The reference is empty chamber + water ( $\sigma = 1.1 \text{ ms/cm}$ ) in vessel.

(4) The chamber was filled by silica suspension (220 nm, 23wt%,  $\sigma = 1.1 \text{ ms/cm}$ ) and then fixed in the vessel, which is filled by water ( $\sigma = 1.1 \text{ ms/cm}$ ) as well. The

reference is chamber filled by water ( $\sigma = 1.1 \text{ ms/cm}$ ) + water ( $\sigma = 1.1 \text{ ms/cm}$ ) in vessel.

The EIT measurement was carried out at 80kHz and 15 mA excitation current. In order to decrease system error and obtain a better result, 8000 frames data were collected and averaged in each measurement. The data were reconstructed using SCG (scaled conjugate gradient) algorithm to get the differential images.

## *2.2. Materials*

Aqueous silica suspensions with different particle size (12 nm, 18 nm, 35 nm, 70 nm, 220 nm, these particle sizes were provided by the manufacturer) were selected for the experiments. The specific surface area of particle is  $80 \text{ m}^2/\text{g}$ , which was measured by BET method and provided by the manufacturer. The silica particle is one of the common colloidal particles, which carries negative charges on the surface and forms an electrical double layer by adsorbing the positive ions on the particle surface. The particle size is in the range of nano-meters (less than 1 micrometer). Due to the surface charge and small size, the particles can be dispersed in the solution to form stable suspensions. The characterization of colloidal particles using EIS basically relies on the electric double layer on the surface of charged particles. Therefore, stabled silica particle suspensions with different particle sizes are very suitable for this study. In addition, the silica particles have approximate spherical shape, so the particle shape has little effect on EIS measurement. Considering the above reasons, the silica particles were chosen in this study. Since the ionic species and

concentrations in the original samples were not given by the manufacturer, in order to get well defined samples, the original samples were firstly de-ionized using mixed bed ion exchange resin (Bio-red), and then diluted to different volume fractions ( $\Phi=4.76\%$ ,  $2.38\%$ ,  $0.476\%$ ,  $0.238\%$ ) using de-ionized water without adding additional electrolyte. The de-ionized process was carried out by adding 4g mixed bed ion exchange resin (Bio-red) into 100g original sample. The suspension was stirred overnight (more than 12 hours) by magnetic stirrer at 150 rpm and finally the de-ionized suspensions can be obtained by filtrating the resin using funnel and water pump.

Since the original silica samples underwent a pre-treatment process before EIS measurement, the particle sizes provided by the manufacturer were no longer applicable. Therefore, the particle size distributions (PSD) of all pre-treated samples were measured using ZetaSizer (Nano Series from Malvern Instruments) before the use in the following analysis. In addition, pH values of pre-treated samples were measured using pH meter (Eutech Instruments pH 300) and zeta potential of suspensions were measured using ZetaSizer (Nano Series from Malvern Instruments).

### **3. Results and discussion**

#### *3.1. Physical properties of SiO<sub>2</sub> nano-particle suspensions*

Since the original silica samples underwent a pre-treatment process before EIS measurement, the physical properties of all pre-treated SiO<sub>2</sub> nano-particle

suspensions, including particle size, zeta potential, pH values and surface charge were measured for the use in the following analysis. The measured particle size distribution curves are shown in Figure 3 for the five suspensions with different particle sizes. The sizes shown in legend were provided by the manufacturer. It can be seen that the aggregation has occurred in all of the samples, since the average particle sizes after pre-treatment is higher than the sizes provided by the manufacturer. The aggregation might be caused by the dilution and de-ionization treatments in the sample preparation. A summary of the average particle sizes (particle diameter) for the five nano-particle suspensions is shown in Table 2. In order to make clear sense of the particle size measured by the ZetaSizer and the size provided by the manufacturer, a notation of  $X^d$  is used to show the measured particle diameter. Here,  $X$  shows the particle diameter measured using the ZetaSizer, and superscript,  $d$ , shows the particle diameter provided by the manufacturer.

The value of double layer thickness,  $\kappa^{-1}$  can be calculated from the ionic concentration by Equation (1) [36], for a symmetric monovalent electrolyte:

$$\kappa^{-1} = \sqrt{\frac{\varepsilon_0 \varepsilon_r k_B T N_A}{2F^2 C_0}} \quad (1)$$

where  $\kappa^{-1}$  is double layer thickness (m),  $k_B$  is Boltzmann constant (J/K),  $N_A$  is Avogadro's constant ( $\text{mol}^{-1}$ ),  $F$  is Faraday constant (C/mol),  $C_0$  is the molar concentration of the electrolyte (mol/litre),  $\varepsilon_0$  is the permittivity of free space (F/m),

$\varepsilon_r$  is the relative dielectric constant of solvent (78.5 for water) and T is the absolute temperature (K).

The electrolyte concentration was estimated from the concentration of H<sup>+</sup> and OH<sup>-</sup> ions that were calculated from pH values. Here, an assumption is used, i.e. the ionic species were entirely removed from the suspensions except H<sup>+</sup> and OH<sup>-</sup> ions after pre-treatment using the mixed bed ion exchange resin. The calculated double layer thickness and the measured pH values of silica suspensions with different particle radius and volume fraction are shown in Table 3. From Table 3, it can be found that all  $\kappa a$  of the samples show thick double layers with small  $\kappa a$  values ( $\kappa a < 1$ ). Here, the definition of  $\kappa a$  value is related with the comparison between the double layer thickness ( $\kappa^{-1}$ ) and particle radius ( $a$ ). At the case of thick double layer, the double layer thickness is larger than the particle radius, e.g.  $\kappa^{-1} > a$ , which can also be represented by  $\kappa a < 1$ . Therefore,  $\kappa a$  value is defined as a parameter which can be used to describe whether the electrical double layer is a thin layer or a thick layer. At the case of  $\kappa a < 1$ , the electrical double layer is a thick layer. When the double layer thickness is much smaller than the particle radius, e.g.  $\kappa^{-1} \ll a$  and  $\kappa a \gg 1$ , the electrical double layer is a thin layer.

The surface charge density can be determined by the measured zeta potential and the double layer thickness by a semi-empirical equation (2) [37]:

$$\sigma_\xi = \varepsilon_r \varepsilon_0 \frac{k_B T}{ze} \kappa \left[ 2 \sinh(z\tilde{\xi}/2) + \frac{4}{\kappa a} \tanh(z\tilde{\xi}/4) \right] \quad (2)$$

where,  $\sigma_\xi$  is the surface charge density (C/m<sup>2</sup>),  $a$  is the particle radius (m),  $\tilde{\xi} = e\xi/k_B T$  is the dimensionless zeta potential,  $z$  is the valence of counterion,  $k_B$  is the Boltzmann constant (J/K),  $T$  is the absolute temperature (K),  $\varepsilon_0$  is the permittivity of free space (F/m),  $\varepsilon_r$  is the relative dielectric constant of solvent (78.5 for water), and  $\kappa$  is Debye-Hückel parameter with dimensions of (length)<sup>-1</sup>(m<sup>-1</sup>), which is the reciprocal of double layer thickness.

Table 4 shows the calculated surface charge density and the measured zeta potential values of silica suspensions. From Table 4, it can be found that the surface charge densities increase with decreasing particle volume fraction. This result might be contributed from the decrease of number of particles in the suspensions, but without significant change in the concentration of H<sup>+</sup>. For most of the samples, it can be found that the surface charge densities increase with decreasing particle radius. This trend could be easily explained by the larger surface area of small particles. An inconsistent tendency on changing of zeta potential with particle size can be observed in Table 4. The possible reason for this result is that zeta potential is not only the function of particle size, but also related to the electrophoretic mobility, double layer thickness and viscosity by the Henry equation[36]:

$$\mu = \frac{2\varepsilon_r \varepsilon_0 \xi}{3\eta} f_1(\kappa a)$$

where  $\mu$  is the electrophoretic mobility (m<sup>2</sup>/s · V) of the particle,  $\xi$  is zeta potential (V),  $\varepsilon_0$  is the permittivity of free space (F/m),  $\varepsilon_r$  is the relative dielectric constant,  $\eta$  is

the dynamic viscosity (Pa·s),  $\kappa$  is Debye-Hückel parameter ( $\text{m}^{-1}$ ) and  $a$  is the particle radius (m).

From Henry equation, it can be found that zeta potential is a parameter which is affected by several parameters. One factor may cause positive effect on zeta potential, but another factor may give negative effect. Therefore, the relationship between particle size and zeta potential shows an inconsistent changing.

### *3.2. Influence of particle size on electrical impedance spectroscopy and relaxation frequency*

#### *3.2.1 Electrical impedance spectra of $\text{SiO}_2$ nano-particle suspensions*

The electrical impedance spectra for the silica nano-particle suspensions with different volume fractions ( $\Phi=4.76\%$ ,  $2.38\%$ ) and various particle size (12nm, 35nm, 70nm, 90nm, 220nm) are shown in Figures 4-5. It can be observed from Figure 4(a) and 5(a) that the impedance real parts at frequencies lower than 10kHz keep constant but decrease with increasing frequency quickly at the frequencies larger than 10kHz. The impedance imaginary parts of the samples show several peaks at the frequency range of 10kHz to 100kHz. This phenomenon shows the dielectric relaxation of the suspensions under the external electric field, which is usually caused by the delay in polarization of the electrical double layer with respect to a changing electric field. This relaxation is often described in terms of permittivity as a function of frequency; so the relationship between the relaxation frequency and particle size/volume fraction will be further discussed by the permittivity curves in the next section.

As shown in Figure 4(a) and 5(a), at low frequency range (<10kHz), the plateaus of impedance real parts increase with increasing particle size when the particle volume fractions were kept constant. It means that the nano-particle suspensions become less conductive with increasing particle size. The conductive property of suspensions is mainly determined by the ionic concentration and particle concentration in the solution and less influenced by the particle size. Therefore, the possible reason might be the lower ionic concentration in the big particle suspensions, which has been represented by the pH values shown in Table 3.

From Figure 4(b) and 5(b), it can be seen that the impedance phase angles change with particle size. For a nano-particle suspension, the phase angle ( $\theta$ ) represents the phase difference between the applied voltage excitation,  $V(t) = V_m \sin(\omega t)$ , and the response current signal,  $I(t) = I_m \sin(\omega t + \theta)$ . Due to the effect of the sinusoidal potential excitation, the polarization of the electric double layer around each particle reverses periodically, but there is a phase lag due to the finite time in the diffusion process of ions along the particle surface trajectory. Therefore, the phase angle is a function of particle size. Since the dielectric relaxation of suspensions occurs around 80kHz, the phase angles of different samples at 80kHz show relative large differences. Thus, the change of phase angle with increasing particle size was studied at a fixed frequency, 80kHz and the result is shown in Figure 6. It can be found that the absolute value of phase angle increases with increasing particle size. The result could be explained by the long time required for the diffusion process of ions along the particle surface in the suspensions with big particles.

### 3.2.2 Permittivity spectra and relaxation frequency

As mentioned in section 3.2.1, the dielectric relaxation of nano-particle suspensions under the alternating electric field can be described in terms of permittivity as a function of frequency. The permittivity curves can be obtained by calculating the permittivity values using electrical impedance data. The frequency dependence of the complex permittivity is usually characterized by two kinds of relaxation mechanisms within the frequency range in this study, 1Hz-32MHz. There are two dielectric relaxation involved,  $\alpha$  relaxation and MWO relaxation[38]. The  $\alpha$  relaxation is also called low frequency dielectric dispersion (LFDD), which usually occurs at lower frequencies (Hz-MHz). The  $\alpha$  relaxation can be explained by volume diffusion model (VDM), which was proposed by Delgado[39-40]. In VDM, the polarisation of the electric double layer is accompanied by a gradient of ionic concentration around the particle surface. The formation of the ionic concentration gradient can be understood easily from the schematic in Figure 7, where a negatively charged spherical particle is under an electric field pointing in the direction from left to right. The counter-ions in the double layer move from the left to the right hand side of the particle and this provokes a tangential electromigration flux of counterions  $J_{es}^+$ . Therefore, the concentration of counter-ions on the right hand side of the particle starts to increase. As for co-ions, they move from the neutral electrolyte to the right hand side of the particle (the outer boundary of the double layer) and provoke a normal electromigration flux of  $J_{en}^-$ . Since the concentration of co-ions in the electrical double layer is much lower than that in the bulk electrolyte solution, the co-ions concentration on the right hand side of

particle also increases. Therefore, an accumulation of both counter-ions and co-ions is formed on the right hand side of the particle and a similar process produces a depletion of both counter-ions and co-ions on the left hand side of the particle. An increment of both the counter-ion and co-ion concentrations means the electrolyte concentration increases at the right hand side of the particle. This phenomenon is called “concentration polarisation”. The concentration gradient of the electrolyte will cause the diffusion of ions along the particle surface. The diffusion is a slow process and need a finite time to be completed. When the frequency of the external electric field becomes high enough, the diffusion process cannot follow the changing of the direction of electric field. At that time, the dielectric relaxation occurs, which is called  $\alpha$  relaxation. For  $\alpha$  dispersion, the relaxation frequency depends on the path length for movement of the counter-ions swarm and therefore is related to the particle size.

The relaxation which occurs in MHz range is called the Maxwell-Wagner-O’Konski relaxation (MWO). It is caused by the different permittivity and conductivity of the particle and the surrounding medium[38]. The relaxation frequency of MWO relaxation is a measure of the time required for charges in the electrolyte solution to recover their equilibrium distribution after ceasing an external perturbation. It is connected with electromigration of ions and will be a faster process than  $\alpha$  dispersion, which is a process controlled by diffusion of the ions in double layer.

The complex permittivity can be converted from the impedance data by the relationships which are shown below.

The impedance  $Z^*$  and complex conductivity  $K^*$  can be expressed by the equations:

$$Z^*(\omega) = Z'(\omega) + iZ''(\omega) \quad (3)$$

$$K^*(\omega) = \sigma'(\omega) + i\sigma''(\omega) \quad (4)$$

where,  $Z'$  and  $Z''$  are the real and imaginary parts of the impedance (both  $Z'$  and  $Z''$  have units of ohm),  $\sigma'$  and  $\sigma''$  are the real and imaginary parts of the complex conductivity (both  $\sigma'$  and  $\sigma''$  have units of S/m),  $\omega$  is frequency (Hz) .

The relationship between the impedance and complex conductivity is given by:

$$K^*(\omega) = \frac{k_c}{Z^*(\omega)} \quad (5)$$

Here,  $k_c$  is the cell constant ( $m^{-1}$ ),  $K^*$  is the complex conductivity (S/m),  $Z^*$  is the impedance (ohm). The cell constant can be calculated via calibration using a standard electrolyte solution. The value of the cell constant is 8.66 for the vessel used in our experiments.

The general presentation of the complex conductivity is given by:

$$K^*(\omega) = \sigma(\omega=0) - i\omega\varepsilon^*(\omega) \quad (6)$$

where,  $\varepsilon^*(\omega)$  is the complex permittivity (F/m),  $\omega$  is frequency (Hz),  $\sigma$  is the DC (direct current) conductivity.

Considering charged particles in suspension, the complex permittivity can be expressed as:

$$\varepsilon^*(\omega) = \varepsilon_0\varepsilon_r^* = \varepsilon_0 \left[ \varepsilon_r'(\omega) + i\varepsilon_r''(\omega) \right] \quad (7)$$

$$K^*(\omega) = \sigma(\omega=0) + \omega\varepsilon_0\varepsilon_r''(\omega) - i\omega\varepsilon_0\varepsilon_r'(\omega) \quad (8)$$

where,  $\varepsilon_0$  is the permittivity of free space (F/m),  $\varepsilon_r^*$  is the complex relative permittivity of suspension,  $\varepsilon_r'$  is the real part of the complex permittivity,  $\varepsilon_r''$  is the imaginary part of the complex permittivity,  $\omega$  is frequency (Hz).

Comparing Equations (4) and (8), we can immediately get the relative permittivity:

$$\varepsilon_r'(\omega) = \frac{-\sigma''(\omega)}{\omega\varepsilon_0} \quad (9)$$

$$\varepsilon_r''(\omega) = \frac{\sigma'(\omega) - \sigma'(\omega = 0)}{\omega\varepsilon_0} \quad (10)$$

where,  $\varepsilon_0$  is the permittivity of free space (F/m),  $\sigma'$  is the real part of the complex conductivity (s/m), and  $\sigma''$  is the imaginary part of the complex conductivity (s/m),  $\omega$  is frequency (Hz).

Figure 8 gives us an idea of the main trends found in the real ( $\varepsilon_r'$ ) and imaginary ( $\varepsilon_r''$ ) components of the permittivity as a function of the frequency of the applied field, for the silica suspensions with different particle size. In order to clearly observe the  $\alpha$  relaxation and MWO relaxation, which usually occur in the kHz to MHz range, permittivity curves show the data from 10kHz to 32MHz. It is easy to identify two different groups of relaxation peaks from these figures. The peaks occur at lower frequency range (100kHz - 1MHz) are due to the  $\alpha$  relaxation, which is associated with the polarisation of the double layer and presents the time taken for the transport of ions at the diffuse double layer over distances of the order of the particle radius. The MWO relaxation occurs at higher frequency (1MHz - 32MHz). There are two groups of peaks which can be found in the MHz range. One is around 1-3MHz and another one around 10MHz. It is believed that the groups of peaks around 1-3MHz represent the Maxwell-Wagner relaxation because it has been proved experimentally by some researchers that MWO relaxation occurs at around several MHz[1,41-42]. The peaks around 10MHz are almost completely overlap for samples with same

particle volume fraction but different particle size, which are probably caused by the effect of parasitic inductance. The high frequency inductive behaviour is usually caused by the physical inductance of the cables, wires, and instrumentation[43]. This phenomenon causes a deviation in EIS measurement, and the EIS data obtained above 10MHz will not be used in the discussion.

The relationship between relaxation frequency  $\omega_\alpha$  and particle size was studied by the imaginary part of complex permittivity spectra in the particle suspensions with different volume fractions ( $\Phi=2.38\%$ ,  $0.476\%$ ,  $0.238\%$ ) and the result is shown in Figure 9. From Figure 8(b) and Figure 9, it can be found that for silica suspensions with relative high volume fraction ( $4.76\%$  and  $2.38\%$ ), the relaxation frequencies obtained from the peak positions, shift to lower frequency range with increasing particle size. However, for the silica suspensions with low volume fractions ( $0.476\%$  and  $0.238\%$ ), the change of relaxation frequency becomes insignificant and irregular with increasing particle size. The possible reason is that with decreasing particle volume fraction, the electrical signal caused by the polarisation of the double layer under the external excitation is getting weak. Therefore, it becomes more difficult to distinguish the change in signal caused by changing of the particle size from the detecting signal.

For dilute suspensions, the frequency at which  $\alpha$  relaxation occurs can be estimated via an equation derived from the model established by Delacey and White[22]:

$$\omega_\alpha \approx \frac{2D}{(a + \kappa^{-1})^2} \quad (11)$$

where,  $\omega_\alpha$  is the  $\alpha$  relaxation frequency (Hz),  $a$  is the particle radius (m),  $\kappa^{-1}$  (m) is

the double layer thickness and  $D$  is the diffusion coefficient of ions ( $\text{m}^2/\text{second}$ ).

The relationship between  $\alpha$  relaxation frequency,  $\omega_\alpha$ , and particle size in 4.76% and 2.38% silica suspensions is shown in Figure 10 (a) and (b), respectively. For both of the figures, the particle radii,  $a$ , are all obtained from the particle sizes measured using the ZetaSizer and the double layer thickness,  $\kappa^{-1}$ , are from Table 3. The  $\alpha$  relaxation frequency as function of particle size can be obtained by the linear fitting of experimental data and the result is shown in Figure 10 by the red line. The fitting equation for  $\text{SiO}_2$  nano-particle suspension with volume fraction of 4.76% and 2.38% can be shown by the equations (12) and (13), respectively:

$$\omega_\alpha \propto (a + \kappa^{-1})^{-0.0925} \quad (12)$$

$$\omega_\alpha \propto (a + \kappa^{-1})^{-0.1022} \quad (13)$$

where,  $\omega_\alpha$  is the  $\alpha$  relaxation frequency (Hz),  $a$  is the particle radius (m) and  $\kappa^{-1}$  (m) is the double layer thickness.

Here two exponents of  $(a + \kappa^{-1})$  do not agree with the value of -2, which is shown in equation (11). The possible reasons could be the thick double layer and the high volume fraction of silica suspensions, 4.76% and 2.38%. The equation (11) is derived for the dilute suspensions. The definition of a dilute suspension is not explicit in the literature. However, in a review paper[44], the authors stated that a volume fraction of 1% should be treated as a concentrated suspension for which the particle interaction makes deviation in using the dilute suspension model. Based on the volume diffusion model (VDM), which can take the electrolyte concentration gradients of neighbouring particles into consideration, in concentrated suspensions, one particle is probably

close to another particle and the double layer polarisation might be affected by changing the diffusion distance of the volume diffusion model[39]. For a dilute suspension, the diffusion distance is the particle size. However, in a concentrated suspension, especially for the colloidal particles with thick double layer, the diffusion distance is lowered by the proximity of the neighbours, so that ions have to move a shorter distance. Therefore by the experimental study in the silica suspensions in this research, deviation between the experimental result and Delancey and White model exists. The proportional relationship between the relaxation frequency and the particle size is still kept, but the exponent of  $(a + \kappa^{-1})$  increases. For the characterization of particle size using  $\alpha$  relaxation frequency, a general equation (14) could be applied, but the exponent,  $n$ , in equation (14) has to be corrected by the experiments.

$$\omega_{\alpha} \propto (a + \kappa^{-1})^{-n} \quad (14)$$

where,  $\omega_{\alpha}$  is the  $\alpha$  relaxation frequency (Hz),  $a$  is the particle radius (m) and  $\kappa^{-1}$  (m) is the double layer thickness.

### *3.3. Influence of particle volume fraction on conductivity increment and relaxation frequency*

The particle volume fraction could affect the conductive property of suspensions, so the impedance real part plays an important role in characterizing particle volume fraction. Figure 11 shows the conductivity increment  $\Delta K'$  relative to background electrolyte conductivity as a function of frequency in silica suspensions with fixed particle size ( $384.5^{220}$  nm) but different concentrations (10.0 wt%, 5.0 wt%, 1.0 wt%, 0.5 wt%).  $\Delta K'$  is defined by the equation (15).

$$\Delta K' = K'_{\text{suspension}} - K'_{\text{background electrolyte}} \quad (15)$$

where,  $\Delta K'$  is the real part of the conductivity increment caused by adding silica particles in the background electrolyte (S/m),  $K'_{\text{suspension}}$  is the real part of the conductivity of suspension (S/m) and  $K'_{\text{background electrolyte}}$  is the real part of the conductivity of background electrolyte (S/m).

It can be found that the conductivity increments  $\Delta K'$  for all of the samples show negative values. It means that the suspensions become less conductive after adding silica particles. However, the highest concentration suspension ( $\Phi= 4.76\%$ ) shows a smallest absolute value of  $\Delta K'$ , i.e. the decrease of conductivity is smallest. This result is contrary to the usual understanding, which is the more particles added, the conductivity of the suspension decreases more. A possible reason, which could explain this phenomenon, is the effect of mobile charge around each particle. If there is no surface charge on the particles, the effect of adding particles to the electrolyte is to remove conductive material and to replace it with non-conductive material. However, if the particles carry surface charge and the double layer contains mobile ions around each particle, the negative effect of adding non-conductive particles can be offset by the positive effect of the extra mobile double layer charge. Consequently, the conductivity increment of suspension becomes less negative as the total mobile double layer charge increases. From Figure 11, it can be seen that  $\Delta K'$  becomes less negative with increasing particle concentration, which means that in the competition between positive double layer contribution and negative particle contribution, the effect of double layer charge on the conductivity increment is more

significant than the effect of impenetrable particles.

The particle concentration not only influences the conductivity but also affects the relaxation frequency of the  $\alpha$  dispersion. The relationship between relaxation frequency  $\omega_\alpha$  and particle volume fraction were studied in the silica suspensions and the experimental results are shown in Figure 12. As Figure 12 shows, the relaxation frequency  $\omega_\alpha$  is not the same for all particle volume fraction. In fact, it increases with volume fraction very significantly. This phenomenon could be explained by the different contribution of small particle and large particle on the reduced diffusion length. With increasing particle concentration, the distance between two particles becomes smaller, and the electrical double layers may partially overlap, especially in the case of thick double layer (the case in our experiments). The increase of relaxation frequency  $\omega_\alpha$  with increasing particle volume fraction can be explained by the decrease in the diffusion length due to the presence of neighbouring particles. The experimental data were analysed by using the linear fitting function and the slope of fitting plots are shown in Figure 12. It can be found that the suspensions with small particles show large slope, which means the effect of particle volume fraction on the relaxation frequency  $\omega_\alpha$  is more significant for small particles than for large particles. This result could be explained by the large total number of particles in the suspension with small particles. If the particle volume fraction keeps constant, the total number of small particles is larger than the total number of large particles. Therefore, the diffusion length due to the close proximity between the particles decreases more significantly in suspensions with small particles, that is, the small particles play a more

predominant role on reduced diffusion length. This result is consistent with other research results based on simulation[44].

#### *3.4. Electrical impedance tomography imaging of silica suspension*

A preliminary experiment was carried out to investigate the electrical impedance tomographic image of silica suspension caused by dielectric relaxation of particles and the results are discussed in this section. Firstly, the position of the chamber in the cylindrical vessel was confirmed using an empty chamber and the result is shown in Figure 13. The blue colour reflects low conductivity and the red colour reflects high conductivity. From Figure 13, a blue colour strip can be observed clearly in the real part image and magnitude part image, which shows the position of the chamber, since the empty chamber has relative low conductivity compared with the water in vessel. In the imaginary part image, the blue colour strip becomes blurring and in the phase angle image, it almost disappears. If the empty chamber is filled by water and fixed in the vessel which is filled by water with same conductivity, the tomography images are shown in Figure 14. At the chamber position, a blue colour, peanut shaped strip can be observed in the real part image and magnitude part image. It can be noticed that although water in the chamber is more conductive than air in the empty chamber, the strip shows blue colour, not red colour. It is probably due to the non-conductive cling film, which was glued on both sides of the chamber. In the imaginary part image and phase angle image, light blue colour can be observed at the chamber position, which represents the difference of dielectric property between water and air (air as reference). In the third experiment, water in the chamber was exchanged by silica

suspension and the reference is the empty chamber plus water in vessel. The EIT result is shown in Figure 15. It can be found that the images in Figure 15 are almost same with those in Figure 14. The impedance real part and magnitude part images are mainly related with the conductivity of the material in chamber, therefore, no significant difference can be observed between Figure 14 (a), (d) and Figure 15 (a), (d) due to the same conductivity value of silica suspension and water. The impedance imaginary part image and phase angle image are related with the dielectric relaxation of the material in chamber. Due to the electrical polarization of double layer on the silica particles, the imaginary part image and phase angle image in Figure 15 should be different with those in Figure 14. However, the difference might be very tiny and couldn't be observed easily from the EIT images. In order to find out the electrical polarization effect caused by silica particles from EIT images, the differential images were reconstructed using SCG algorithm and the result is shown in Figure 16. It can be found that the blue colour strip at the chamber position disappears in figure 16(a) and (d), which means there is no difference on conductivity between the silica suspension and water. It is consistent with the real situation. In the imaginary part image and phase angle image, light blue colour and red colour strips at the upper right corner can be observed, which represent small differentiation on the dielectric property caused by the electrical polarization of double layer on the particles. However, the position of colour strips is not exactly identical with the chamber position shown in Figure 13. The possible reason for this phenomenon could be related to the inaccuracy of measurement on this tiny differentiation due to the limitation from

hardware and the data reconstruction algorithm. In order to measure the tiny differentiation, the improvement on both hardware and theoretical model could be considered. From the aspect of hardware, the instrumentation should be improved to decrease the effect of common mode voltage in the electrical impedance tomography imaging measurement, since it is known that the common mode voltage effect is the main source of instrumentation error. From the aspect of the evaluation to the theoretical model, an equivalent circuit model based on RC network (RC refers to number of resistors and capacitors respectively) could be developed to simulate the electrical property of particle suspensions in a two-dimensional phantom. The RC network equivalent circuit model may further be employed to evaluate the reconstruction quality and the measurement accuracy for the tiny differentiation in EIT test.

The current study has demonstrated that electrical impedance spectroscopy/tomography could be a method of particle characterization due to the relationship between the particle properties (e.g. the size, concentration) and the electrical impedance parameters. However, there is still a distance from the fundamental study to its real application because of some technical challenges. To resolve the challenges, some future work could be considered. For example, the methods will be applied to other kinds of particles to seek commonality from comparing these results. The comparison across the different materials allows for a better verification and improvement of the method. As it is shown in figures 4(b) and 5(b), the largest values of phase angle ( $|\theta|$ ) occur at about 1MHz in these tests. The

differentiation between particle suspension and reference (water) could become larger and be easily measured if the measurement in EIT could be operated at 1MHz. Therefore, as one of the future work, the operating frequency of instrument will be increased in conjunction with more effective and rapid solution methods on excitation and measurement for imaging the spatial and temporal distribution of particle characteristics in process dynamic applications.

#### 4. Conclusion

1) The dielectric relaxation of SiO<sub>2</sub> nano-particle suspensions was studied using electrical impedance spectra and permittivity spectra. The influences of particle size on electrical impedance spectroscopy and relaxation frequency are analyzed and discussed in detail. The phase angle is a function of particle size and at a fixed frequency, the absolute value of phase angle increases with increasing particle size.

2) The relaxation frequencies of  $\alpha$  relaxation shown in the permittivity spectra are a function of particle size changing proportionally with  $(a + \kappa^{-1})^{-n}$  ( $n$  equals 0.344 for 4.76% suspension and 0.308 for 2.38% suspension). The exponent  $n$  is smaller than the one in dilute suspensions ( $n=2$ ), which is possibly due to decreasing of diffusion distance of ions around the particles in concentrated suspensions with thick double layer.

3) The conductivity increment,  $\Delta K'$ , becomes less negative with increasing particle volume fraction, because the positive effect of double layer charge on the conductivity

increment is more significant than the negative effect of impenetrable particles. The relaxation frequency of  $\alpha$  dispersion increases with increasing particle volume fraction.

4) An experimental method based on differential EIT imaging between the silica particle suspension and water (with same conductivity value) and sample holder were established. Results show the influence of nano-particle suspension in respective images. The strip with low conductivity (blue colour in Figure16) at the chamber position disappears in the impedance real part image and the magnitude part image due to the same conductivity value between the disperse phase (silica suspension) and reference (water). On the imaginary part image and the phase angle image, small differences on the values of impedance imaginary part and phase angle can be found, which may represent a small differentiation on the dielectric property caused by the electrical polarization of double layer on the particle surface.

## **5. Acknowledgements**

Authors would like to thank Fuso Chemical Co., Ltd., Japan who provided the colloidal silica suspensions for the research. This work was supported by National Natural Science Foundation of China (No. 51406235); Science Foundation of China University of Petroleum, Beijing (No. 2462013YJRC030) and University of Leeds.

**Reference:**

- [1] J.R. Macdonald, Impedance spectroscopy, emphasizing solid materials and systems, A Wiley-Interscience publication, **1987**, 1-26.
- [2] K.S. Zhao and K.J. He, Dielectric relaxation of suspensions of nanoscale particles surrounded by a thick electric double layer, *Phys. Rev. B: Condens. Matter Mater. Phys.* 74 (2006) 1-10.
- [3] S.S. Dukhin and V.N. Shilov, Kinetic aspects of electrochemistry of disperse systems .2. Induced dipole-moment and the nonequilibrium double-layer of a colloid particle, *Adv. Colloid Interface Sci.* 13 (1980) 153-195.
- [4] R.W. O'Brien, The response of a colloidal suspension to an alternating electric-field, *Adv. Colloid Interface Sci.* 16 (1982) 281-320.
- [5] K.H. Lim and E.I. Franses, Electrical-properties of aqueous dispersions of polymer microspheres, *J. Colloid Interface Sci.* 110 (1986) 201-213.
- [6] P. Mougín, A. Thomas, D. Wilkinson, G. White, K.J. Roberts, N. Herrmann, R. Jack, R. Tweedie, On-line monitoring of a crystallization process, *AIChE J.* 49 (2003) 373-378.
- [7] S. Schorsch, T. Vetter, M. Mazzotti, Measuring multidimensional particle size distributions during crystallization, *Chem. Eng. Sci.* 77 (2012) 130-142.

- [8] E. Kougoulos, A.G. Jones, M.W. Wood-Kaczmar, Modelling particle disruption of an organic fine chemical compound using Lasentec focussed beam reflectance monitoring (FBRM) in agitated suspensions, *Powder technol.* 155 (2005) 153-158.
- [9] Z. Ma, H.G. Merkus, J.G.A. E de Smet, C. Heffels, B. Scarlett, "New developments in particle characterization by laser diffraction: size and shape", *Powder Technol.* 111, (1-2) (2000) 66-78.
- [10] A. Abbas, D. Nobbs, J.A. Romagnoli, Investigation of on-line optical particle characterization in reaction and cooling crystallization systems. Current state of the art, *Meas. Sci. Technol.* 3 (2002) 349-356.
- [11] N. Kail, H. Briesen, W. Marquardt, Analysis of FBRM measurements by means of a 3D optical model, *Powder Technol.* 185 (2008) 211-222.
- [12] C. Tontrup, F. Gruy, Light backscattering by fine non-absorbing suspended particles, *Powder Technol.* 107 (2000) 1-12.
- [13] J.C. De Anda, X.Z. Wang, X. Lai, K.J. Roberts, K.H. Jennings, M.J. Wilkinson, D. Watson, D. Roberts, Real-time product morphology monitoring in crystallization using imaging technique, *AIChE J.* 51 (2005) 1406-1414.
- [14] W. Yu, K. Erickson, Chord length characterization using focused beam reflectance measurement probe-methodologies and pitfalls, *Powder Technol.* 185 (2008) 24-30.

- [15] P.J. Holden, M. Wang, R. Mann, F.J. Dickin, R.B. Edwards, Imaging stirred-vessel macromixing using electrical resistance tomography, *AICHE J.* 44 (1998) 780-790.
- [16]. M. Wang, A. Dorward, D. Vlaev, R. Mann, Measurements of gas-liquid mixing in a stirred vessel using electrical resistance tomography (ERT), *Chem. Eng. J.* 77 (2000) 93-98.
- [17] M. Wang, W. Yin, N. Holliday, A highly adaptive electrical impedance sensing system for flow measurement", *Meas. Sci. Technol.* 13 (2002) 1884-1889.
- [18] R.A. Williams, X. Jia, S.L. Mckee, Development of slurry mixing models using resistance tomography, *Powder Technol.* 87 (1996) 21-27.
- [19] F. Dickin and M. Wang, Electrical resistance tomography for process applications, *Meas. Sci. Technol.* 7 (1996) 247-260.
- [20] M. Wang, Inverse solutions for electrical impedance tomography based on conjugate gradients methods, *Meas. Sci. Technol.* 13 (2002) 101-117.
- [21] F. Carrique, E. Ruiz-Reina, F.J. Arroyo, M.L. Jimenez, A.V. Delgado, Dielectric response of a concentrated colloidal suspension in a salt-free medium, *Langmuir*, 24 (2008) 11544-11555.

- [22] E.H.B. Delacey and L.R. White, Dielectric response and conductivity of dilute suspensions of colloidal particles, *J. Chem. Soc., Faraday Trans.* 77 (1981) 2007-2039.
- [23] J. Kijlstra, H.P. Vanleeuwen, J. Lyklema, Low-frequency dielectric-relaxation of hematite and silica sols, *Langmuir*, 9 (1993) 625-1633.
- [24] H.P. Schwan, G. Schwarz, J. Maczuk, H. Pauly, On low-frequency dielectric dispersion of colloidal particles in electrolyte solution, *J. Phys. Chem.* 66 (1962) 2626-2635.
- [25] M. Thambidurai, N. Muthukumarasamy, Dhayalan Velauthapillai, S. Agilan, R. Balasundaraprabh, Impedance spectroscopy and dielectric properties of cobalt doped CdS nanoparticles, *Powder Technol.* 217 (2012) 1-6.
- [26] A.V. Delgado, F. Gonzalez-Caballero, R.J. Hunter, L.K. Koopal, J. Lyklema, Measurement and interpretation of electrokinetic phenomena, *J. Colloid Interface Sci.* 309 (2007) 194-224.
- [27] B.B. Sauer, R.S. Stock, K.H. Lim, W.H. Ray, Polymer latex particle-size measurement through high-speed dielectric-spectroscopy, *J. Appl. Polym. Sci.* 39 (1990) 2419-2441.
- [28] M. Louge, M. Opie, Measurements of the effective dielectric permittivity of suspensions, *Powder technol.* 62 (1990) 85-94.

[29] F.J. Arroyo, F. Carrique, T. Bellini, A.V. Delgado, Dielectric dispersion of colloidal suspensions in the presence of stern layer conductance: Particle size effects, *J. Colloid Interface Sci.* 210 (1999) 194-199.

[30] S.J.R. Simons, R.A. Williams, particle-size measurement using noninvasive dielectric sensors, *Powder Technol.* 73 (1992) 85-90.

[31] Y. Zhao, M. Wang, R.B. Hammond, Characterisation of nano-particles in colloids: relationship between particle size and electrical impedance spectra, *J. Nanosci. Nanotechnol.* 13 (2013) 808-812.

[32] Y. Zhao, M. Wang, R.B. Hammond, Characterisation of crystallisation processes with electrical impedance spectroscopy, *Nucl. Eng. Des.* 241 (2011) 1938-1944.

[33] F. Carrique, F.J. Arroyo and A.V. Delgado, Effect of size polydispersity on the dielectric relaxation of colloidal suspensions: A numerical study in the frequency and time domains, *J. Colloid Interface Sci.* 206 (1998) 569-576.[34] F.J. Arroyo, F. Carrique, T. Bellini and A.V. Delgado, Dielectric dispersion of colloidal suspensions in the presence of stern layer conductance: Particle size effects, *J. Colloid Interface Sci.* 210(1999) 194-199.

[35] Carrique, F., Ruiz-Reina, E., Arroyo, F. J., Jimenez, M. L. and Delgado, A. V., "Dielectric response of a concentrated colloidal suspension in a salt-free medium", *Langmuir*, vol. 24, 11544-11555, (2008)

[36] R.J. Hunter, *Foundations of colloid science*, Oxford University Press, 2001.

- [37] A.V. Delgado, F. Gonzalezcaballero, J.M. Bruque, On the zeta-potential and surface-charge density of montmorillonite in aqueous-electrolyte solutions, *J. Colloid Interface Sci.* 113 (1986) 203-211.
- [38] L.M. Dudley, S. Bialkowski, D. Or, C. Junkermeier, Low frequency impedance behavior of montmorillonite suspensions: Polarization mechanisms in the low frequency domain, *Soil. Sci. Soc. Am J.* 67 (2003) 518-526.
- [39] A.V. Delgado, F.J. Arroyo, F. Gonzalez-Caballero, V.N. Shilov, Y.B. Borkovskaya, The effect of the concentration of dispersed particles on the mechanisms of low-frequency dielectric dispersion (lfdd) in colloidal suspensions, *Colloids Surf., A* 140 (1998) 139-149.
- [40] J. Lyklema, M.M. Springer, V.N. Shilov, S.S. Dukhin, The relaxation of the double-layer around colloidal particles and the low-frequency dielectric-dispersion .3. Application of theory to experiments, *J Electroanal. Chem.* 198, (1986) 19-26.
- [41] C. Ballario, A. Bonincontro, C. Cametti, Dielectric dispersions of colloidal particles in aqueous suspensions with low ionic-conductivity, *J. Colloid Interface Sci.* 54 (1976) 415-423.
- [42] G. Blum, H. Maier, F. Sauer, H.P. Schwan, Dielectric-relaxation of colloidal particle suspensions at radio frequencies caused by surface conductance, *J. Phys. Chem.* 99 (1995) 780-789.

[43] C.Y. He, B.G. Liu, M. Li, C.X. Gao, Alternating current impedance spectroscopy measurement under high pressure, *Rev. Sci. Instrum.* 82 (2011), 015104-015104-4.

[44] C. Grosse, A.V. Delgado, Dielectric dispersion in aqueous colloidal systems, *Curr. Opin. Colloid Interface Sci.* 15 (2010) 145-159.

Table 1: Dimensions of the chamber and EIT vessel

Experimental setup	Dimensions (mm)
Chamber	125 height, 62 width, 20 length
Height of vessel	25
Internal diameter of cylindrical vessel	14.8

Table 2: Summary of the particle sizes for SiO<sub>2</sub> nano-particle suspensions

Particle diameter provided by vender, d(nm),(d=2a, a is particle radius)	Average particle diameter after pre-treatment, d(nm),( d=2a, a is particle radius)
12	13.5
35	91.3
70	190.1
90	199.7
220	384.6

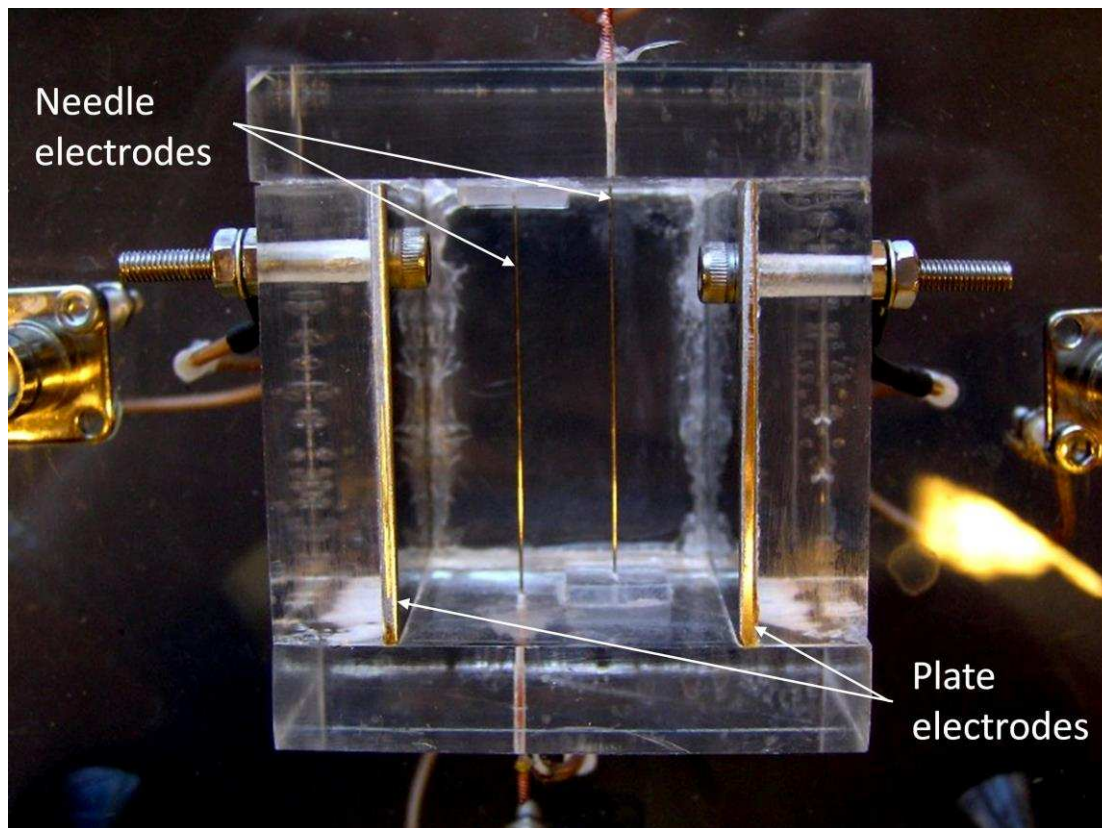
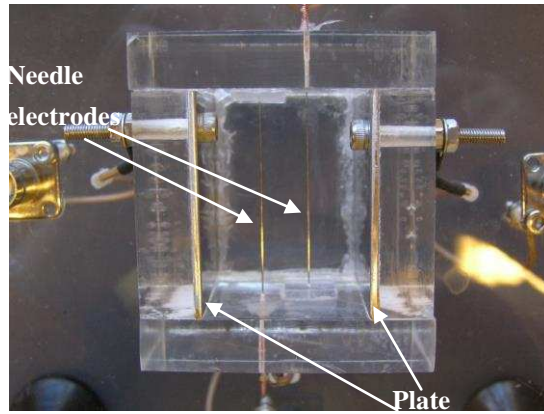
Table 3: The double layer thickness ( $\kappa^{-1}$ ) and pH values of SiO<sub>2</sub> nano-particle suspensions

Samples		Double layer thickness, $\kappa^{-1}$ (nm)	pH value	$\kappa a$
particle diameter, d=2a (nm)	volume fraction, $\phi$ (%)			
13.54	4.76	59.28	4.58	0.114
91.28	4.76	228.01	5.75	0.200
190.1	4.76	613.6	6.61	0.155
199.7	4.76	799.6	6.84	0.125
384.6	4.76	606.5	6.60	0.317
13.54	2.38	70.45	4.73	0.096
91.28	2.38	290.33	5.96	0.157
190.1	2.38	498.7	6.43	0.190
199.7	2.38	642.57	6.65	0.155
384.6	2.38	696.4	6.72	0.276
13.54	0.476	99.55	5.03	0.068
91.28	0.476	357.2	6.14	0.128
190.1	0.476	449.64	6.34	0.211
199.7	0.476	439.63	6.32	0.227
384.6	0.476	429.4	6.30	0.448
13.54	0.238	190.08	5.59	0.036
91.28	0.238	307.66	6.01	0.148
190.1	0.238	373.63	6.15	0.254
199.7	0.238	405.57	6.25	0.246
384.6	0.238	510.59	6.45	0.377

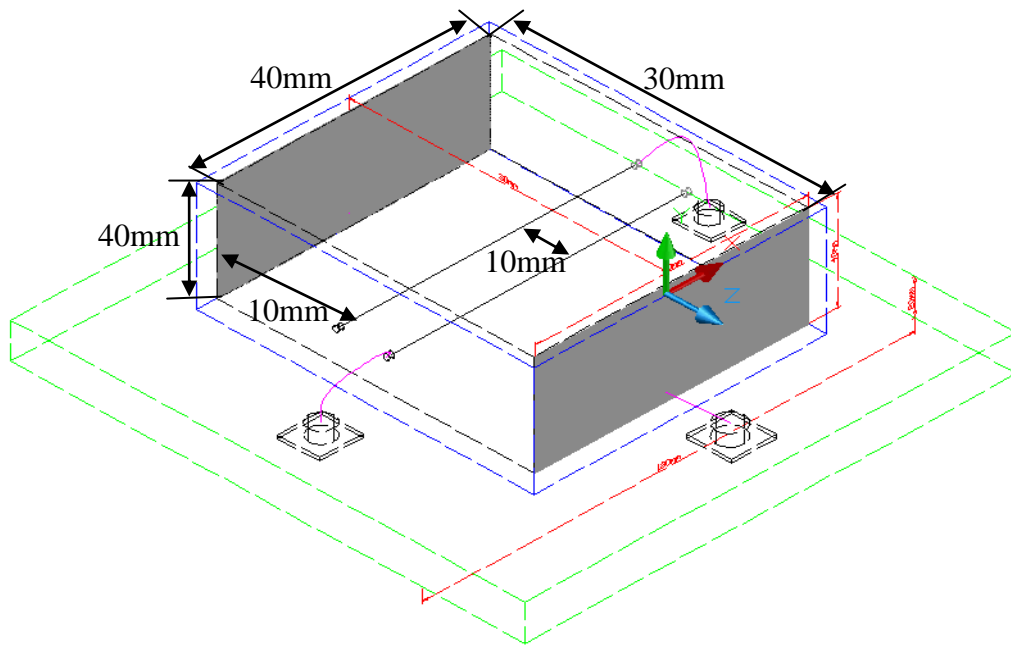
Table 4: The surface charge density ( $\sigma_\xi$ ) and zeta potential ( $\xi$ ) values of SiO<sub>2</sub> nano-particle suspensions

Samples		Zeta potential, $\xi$ (mV)	Surface charge density, $\sigma_\xi$ ( $\mu\text{C}/\text{cm}^2$ )
particle diameter, d (nm)	volume fraction, $\phi$ (%)		
13.54	4.76	-5.0	0.0427
91.28	4.76	-17.2	0.0177
190.1	4.76	-24.1	0.0170
199.7	4.76	-16.6	0.0103
384.6	4.76	-1.1	0.00045
13.54	2.38	-10.1	0.1127
91.28	2.38	-22.1	0.0384
190.1	2.38	-30.0	0.0256
199.7	2.38	-29.9	0.0236
384.6	2.38	-38.4	0.0174
13.54	0.476	-18.0	0.3379
91.28	0.476	-20.0	0.0505
190.1	0.476	-29.1	0.0285
199.7	0.476	-25.6	0.0233
384.6	0.476	-35.4	0.0186
13.54	0.238	-21.8	0.3982
91.28	0.238	-24.6	0.0545
190.1	0.238	-19.4	0.0216
199.7	0.238	-46.6	0.0428
384.6	0.238	-32.7	0.0150

Figure 1



(a) photography of the vessel



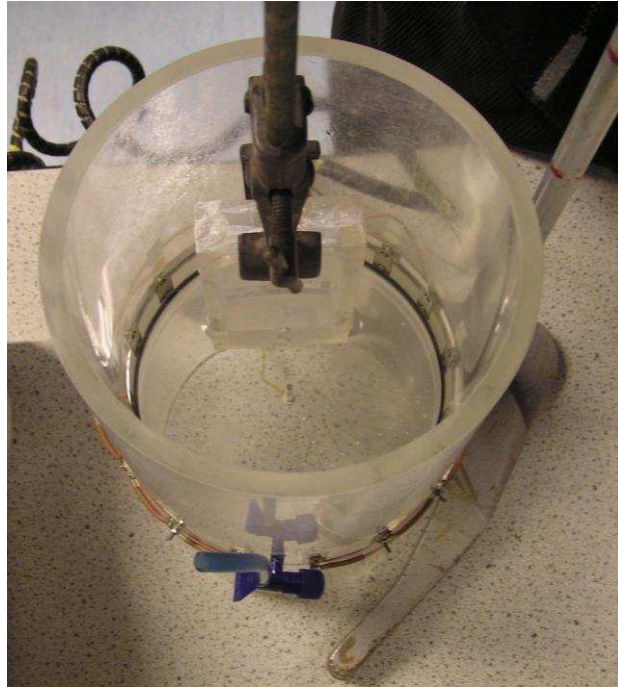
(b) drawing picture and dimensions of vessel

Figure 1: Photograph and drawing picture of the vessel with the four-electrode sensor

Figure 2



(a) Perspex chamber as a housing for silica suspension



(b) the chamber fixed in the cylindrical vessel

Figure 2: Photograph of the experimental set-up for EIT measurement

Figure 3

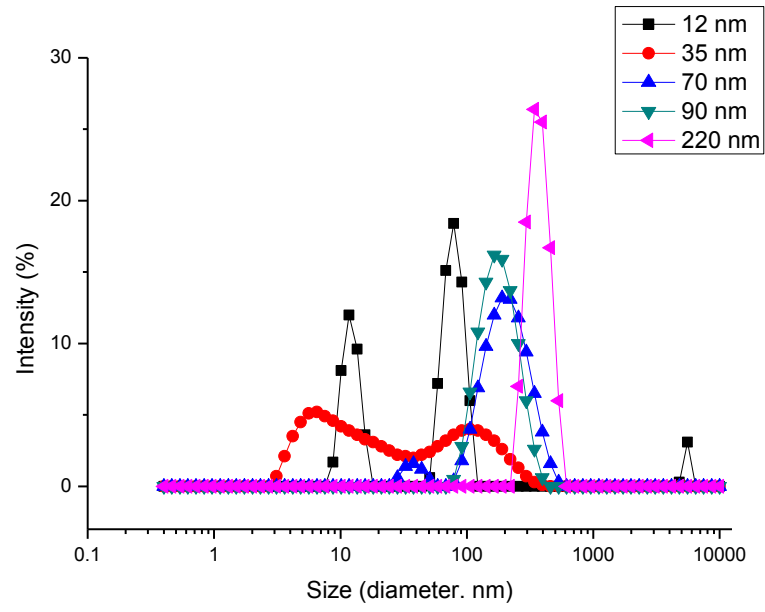
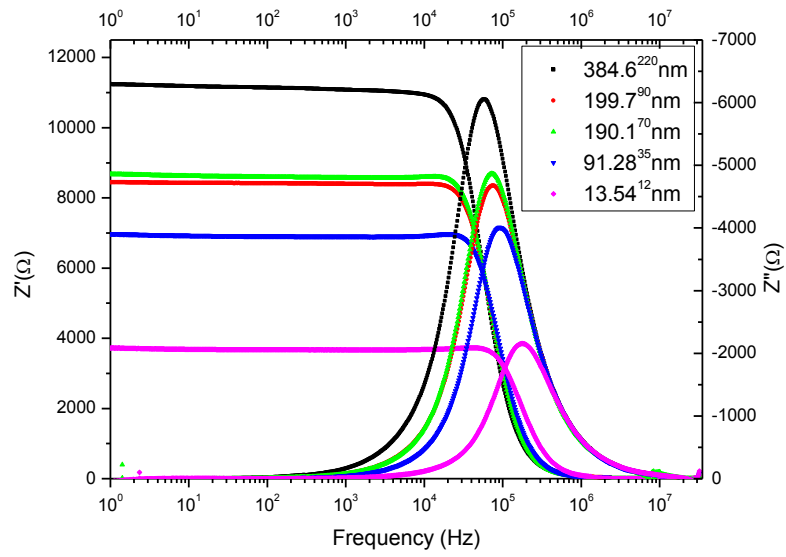
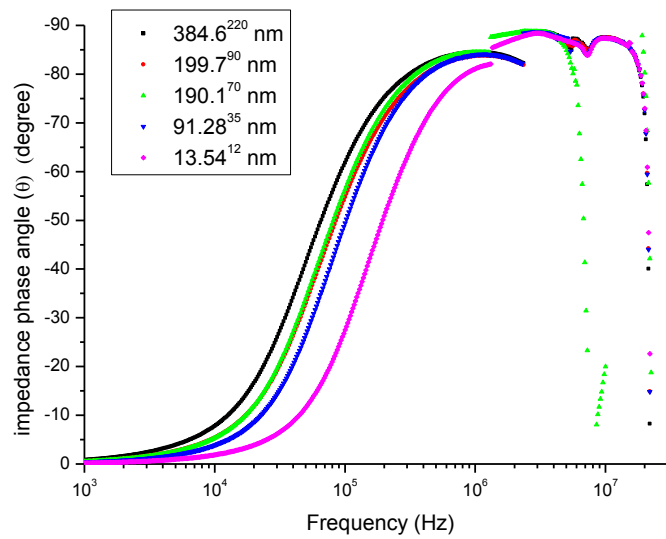


Figure 3: Particle size distribution of SiO<sub>2</sub> nano-particle suspensions

Figure 4



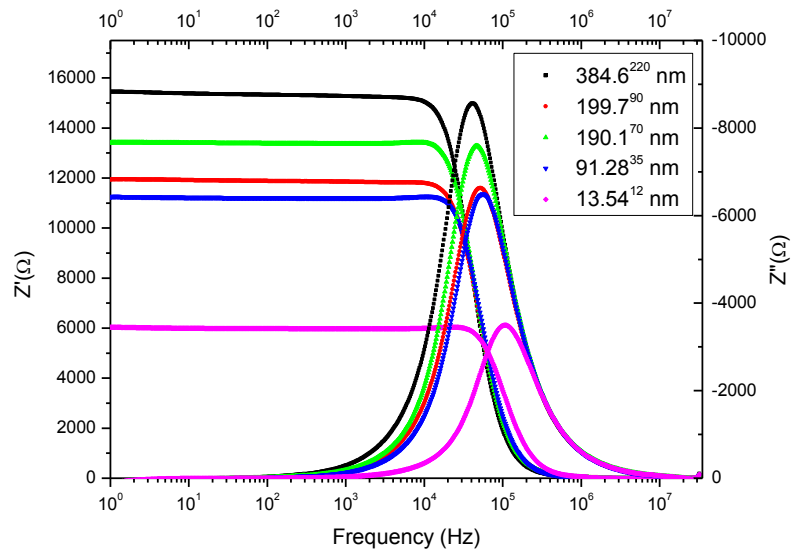
(a)



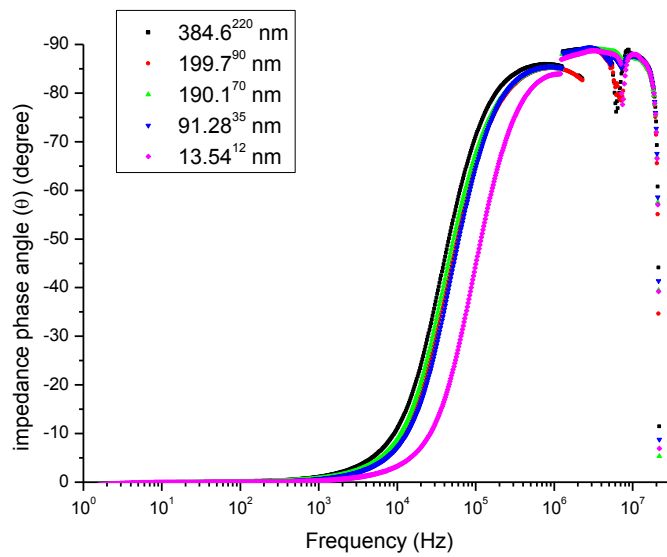
(b)

Figure 4: Impedance spectra for silica suspensions ( $\Phi=4.76\%$ ) with different particle size ( $13.54^{12}$  nm,  $91.28^{35}$  nm,  $190.1^{70}$  nm,  $199.7^{90}$  nm,  $384.6^{220}$  nm); (a) real and imaginary part vs. frequency; (b) phase angle vs. frequency

Figure 5



(a)



(b)

Figure 5: Impedance spectra for silica suspensions ( $\Phi=2.38\%$ ) with different particle size ( $13.54^{12}$  nm,  $91.28^{35}$  nm,  $190.1^{70}$  nm,  $199.7^{90}$  nm,  $384.6^{220}$  nm); (a) real and imaginary part vs. frequency; (b) phase angle vs. frequency

Figure 6

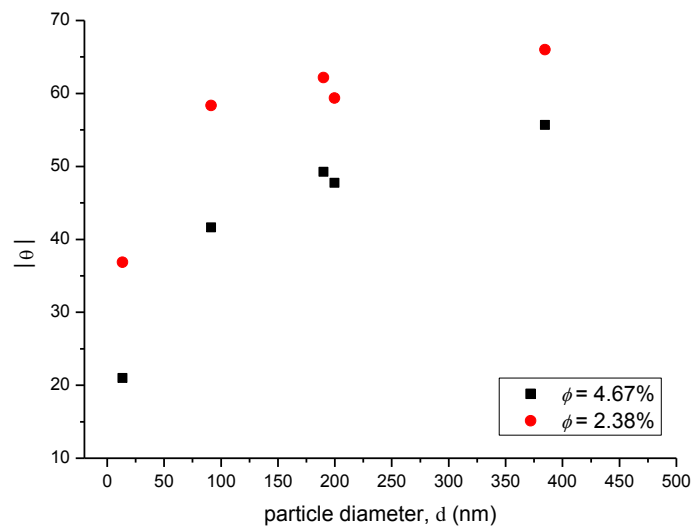


Figure 6: Absolute value of phase angle ( $|\theta|$ ) at 80kHz as function of particle size (d) for silica suspensions ( $\phi=4.67\%$  and  $2.38\%$ )

Figure 7

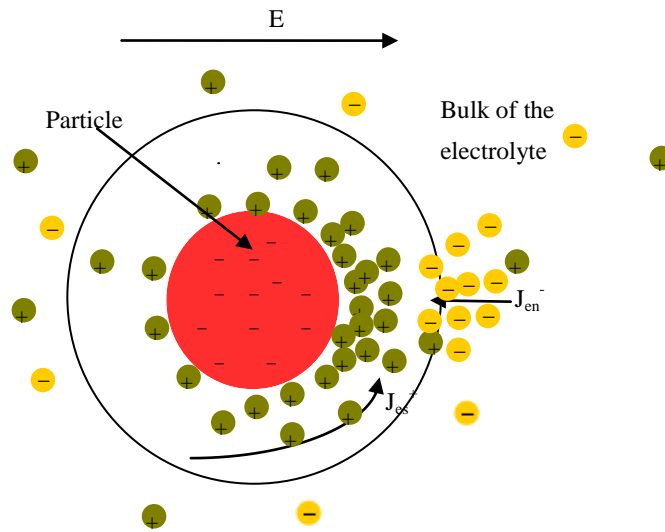
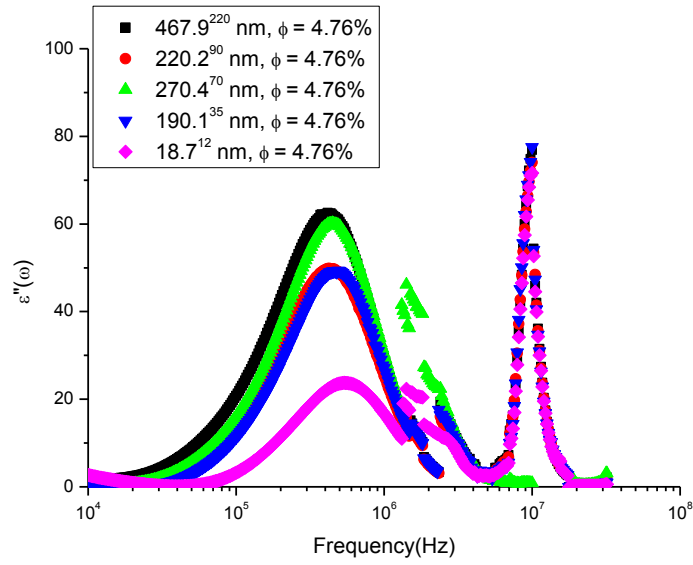
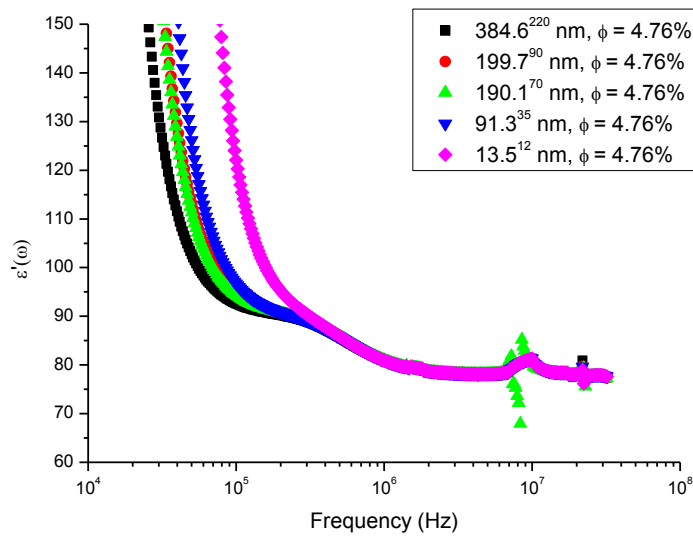


Figure 7: Schematic of the generation of electrolyte concentration gradient responsible for  $\alpha$  relaxation for a negatively charged particle ( $E$  is the applied external electrical field,  $J_{es}^+$  is the tangential electromigration flux of counterions,  $J_{en}^-$  is the normal electromigration flux of the co-ions)

Figure 8



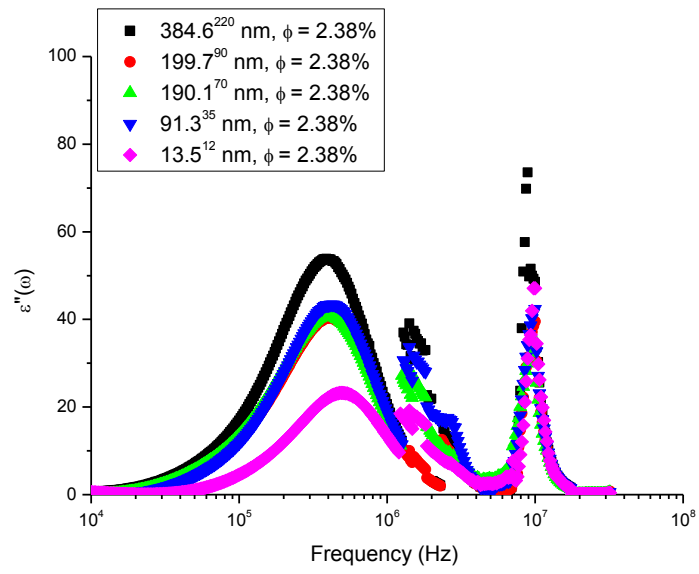
(a)



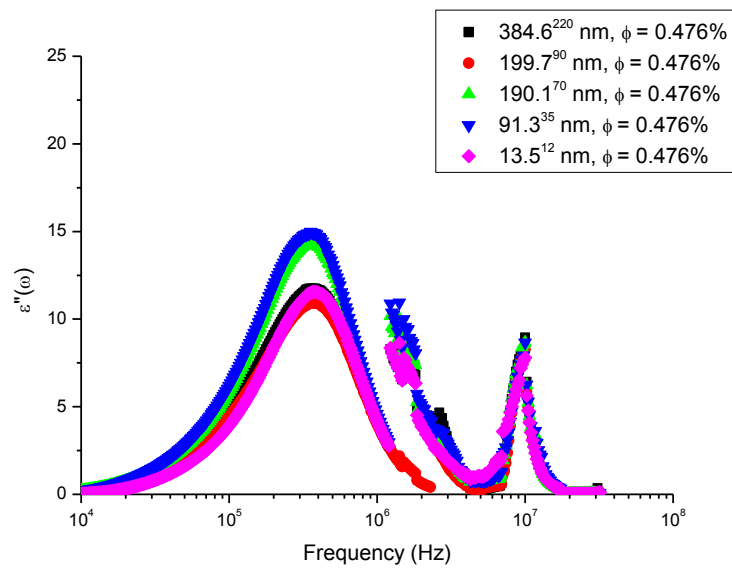
(b)

Figure 8: Frequency response of the (a) real; and (b) imaginary part of complex permittivity of silica suspensions ( $\Phi = 4.76\%$ ) for different particle size indicated.

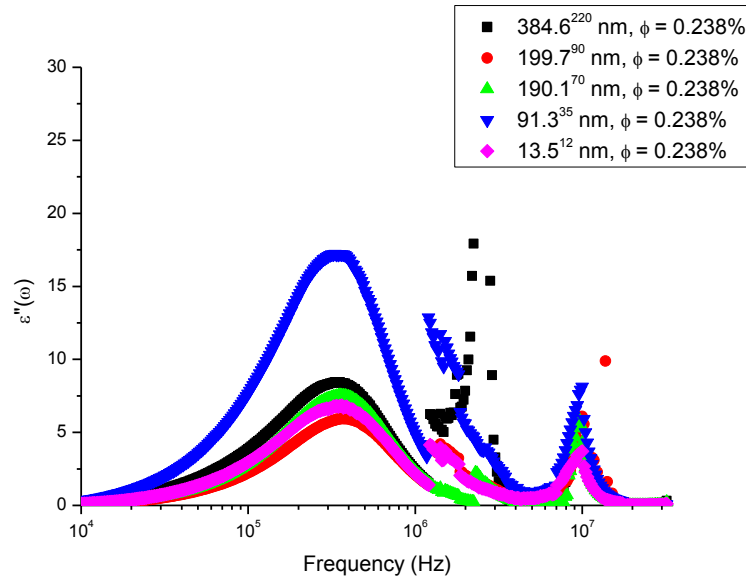
Figure 9



(a)



(b)



(c)

Figure 9: The imaginary part of complex permittivity spectra for silica suspensions with different particle size (a)  $\phi = 2.38\%$ ; (b)  $\phi = 0.476\%$ ; (c)  $\phi = 0.238\%$

Figure 10

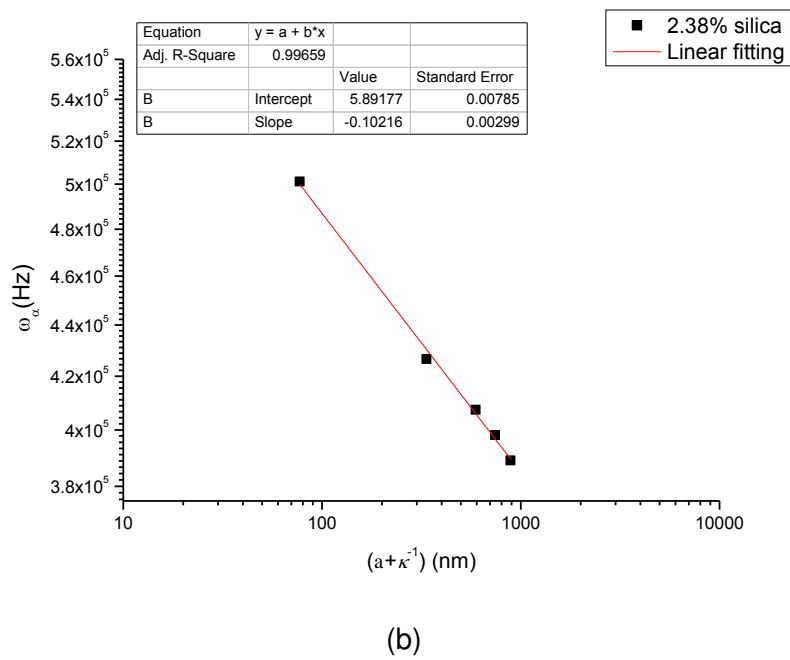
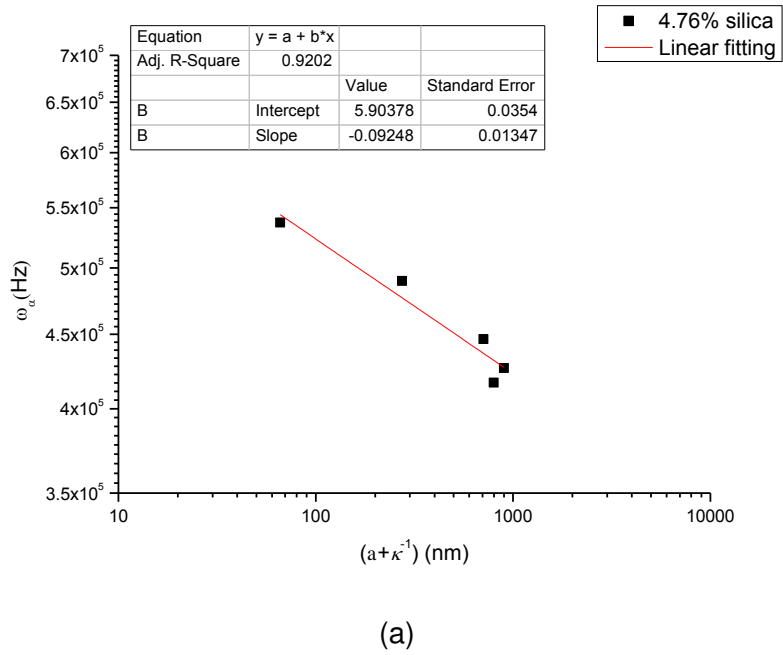


Figure 10: The relaxation frequency  $\omega_\alpha$  is plotted against  $(a + \kappa^{-1})$  for silica suspensions (a)  $\Phi = 4.76\%$ ; (b)  $\Phi = 2.38\%$ .

Figure 11

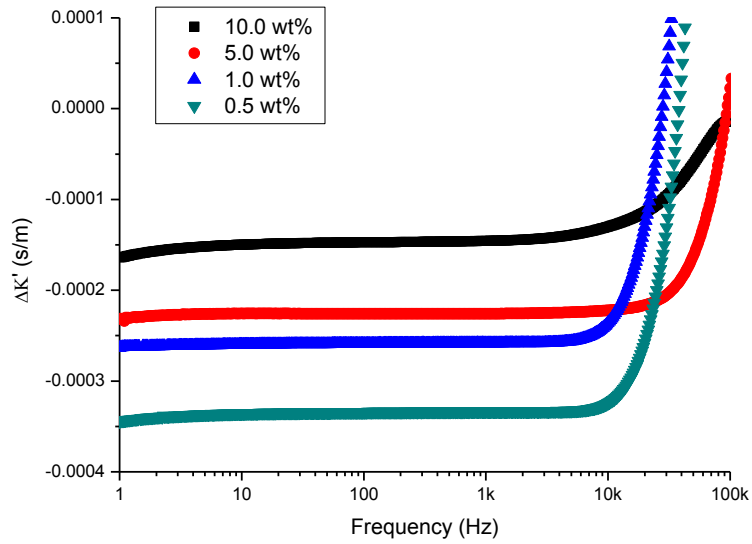
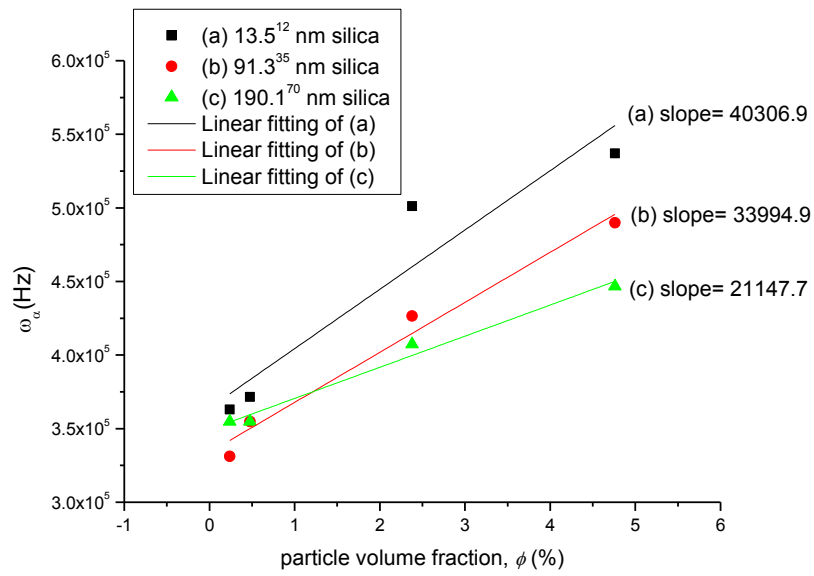
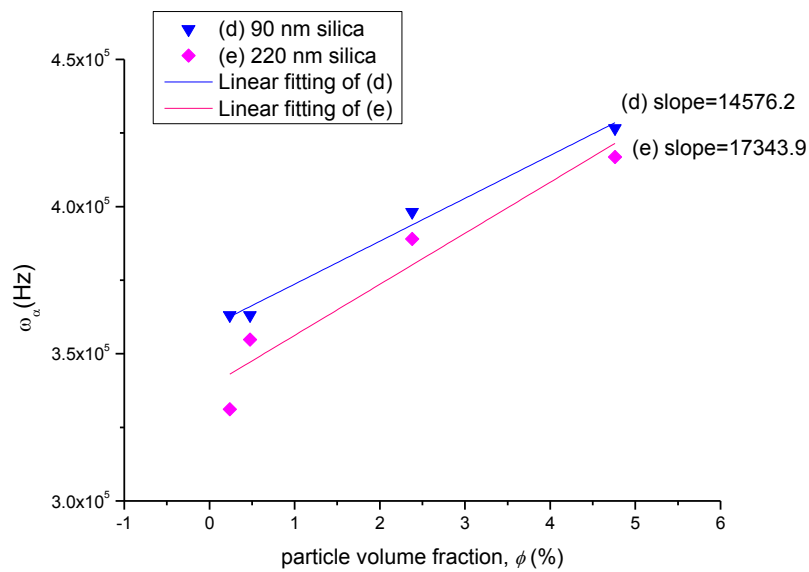


Figure 11: Conductance increment  $\Delta K'$  relative to background electrolyte conductance as function of frequency for silica suspensions ( $384.5^{220}$  nm) with different particle volume fractions ( $\phi = 4.76\%$ ,  $2.38\%$ ,  $0.476\%$ ,  $0.238\%$ )

Figure 12



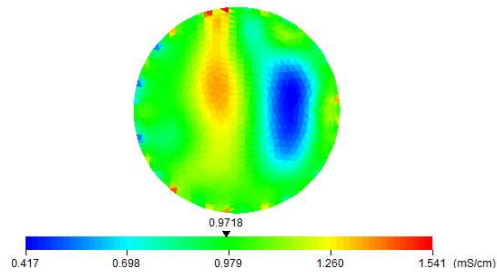
(a)



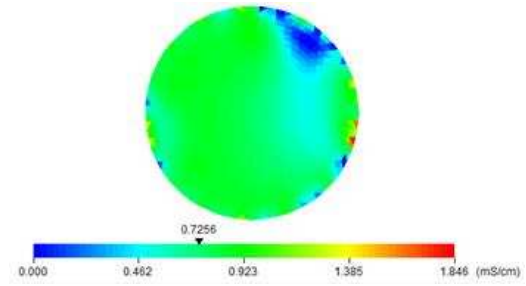
(b)

Figure 12: The relaxation frequency  $\omega_\alpha$  as a function of volume fraction ( $\phi$ ) for silica suspensions: (a) small particles (13.5<sup>12</sup> nm, 91.3<sup>35</sup> nm, 190.1<sup>70</sup> nm); (b) large particles (199.7<sup>90</sup> nm, 384.6<sup>220</sup> nm).

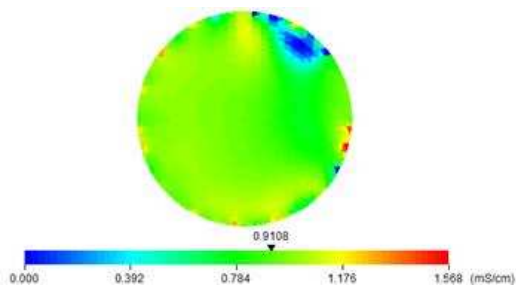
Figure 13



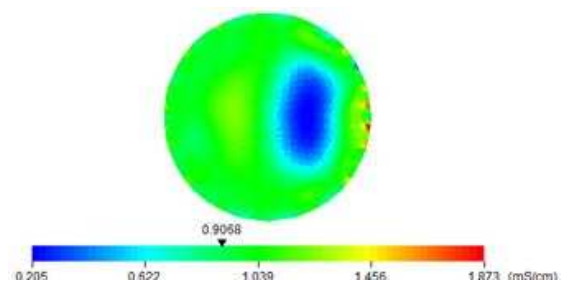
(a) real part image



(b) imaginary part image



(c) phase angle ( $\tan(\theta)$ ) image



(d) magnitude part image

Figure 13: EIT images of an empty chamber in a vessel (reference is water): (a) real part image, (b) imaginary part image, (c) phase angle ( $\tan(\theta)$ ) image, and (d) magnitude part image

Figure 14

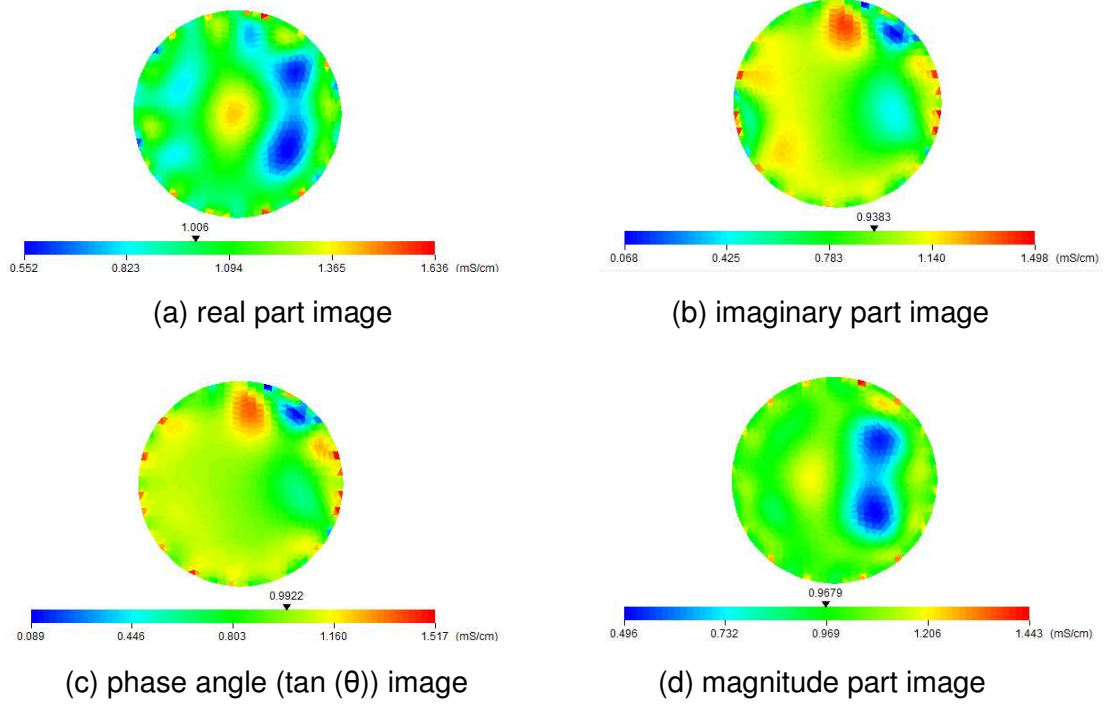


Figure 14: EIT images of chamber (filled with water) in a vessel (reference is the empty chamber fixed in the vessel): (a) real part image, (b) imaginary part image, (c) phase angle ( $\tan(\theta)$ ) image, and (d) magnitude part image

Figure 15

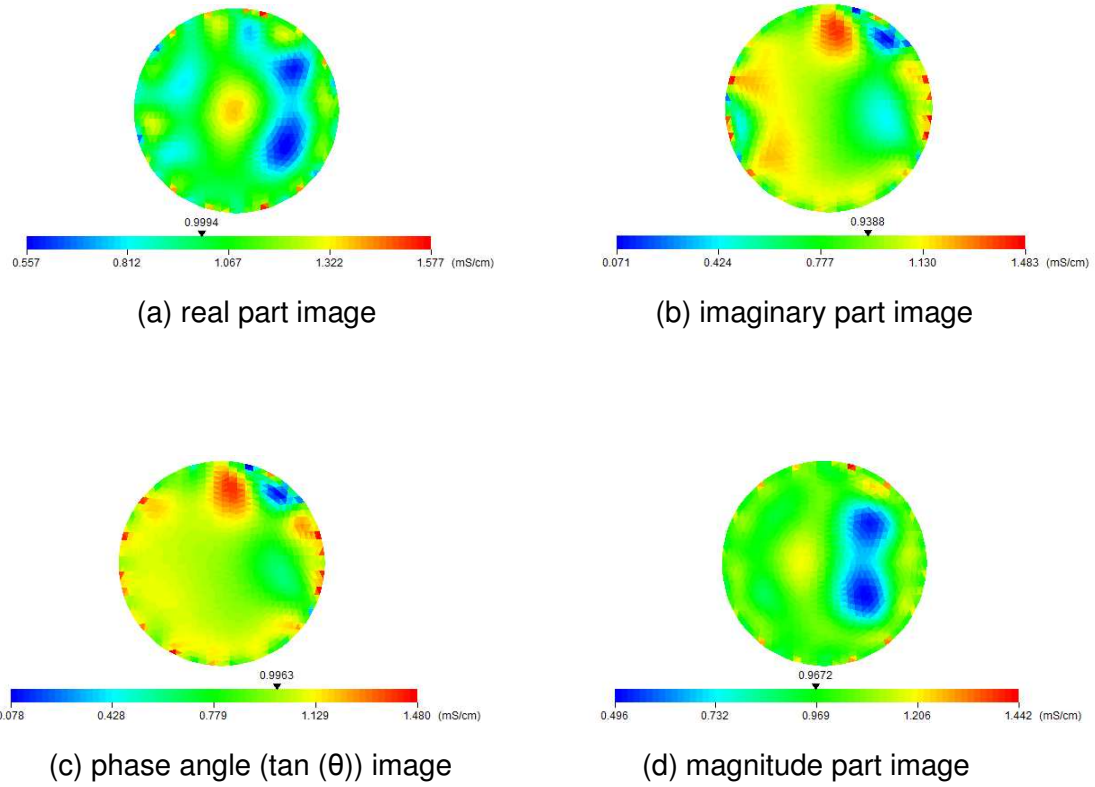


Figure 15: EIT images of silica suspension filled in a chamber (reference is the empty chamber in the vessel): (a) real part image, (b) imaginary part image, (c) phase angle ( $\tan(\theta)$ ) image, and (d) magnitude part image

Figure 16

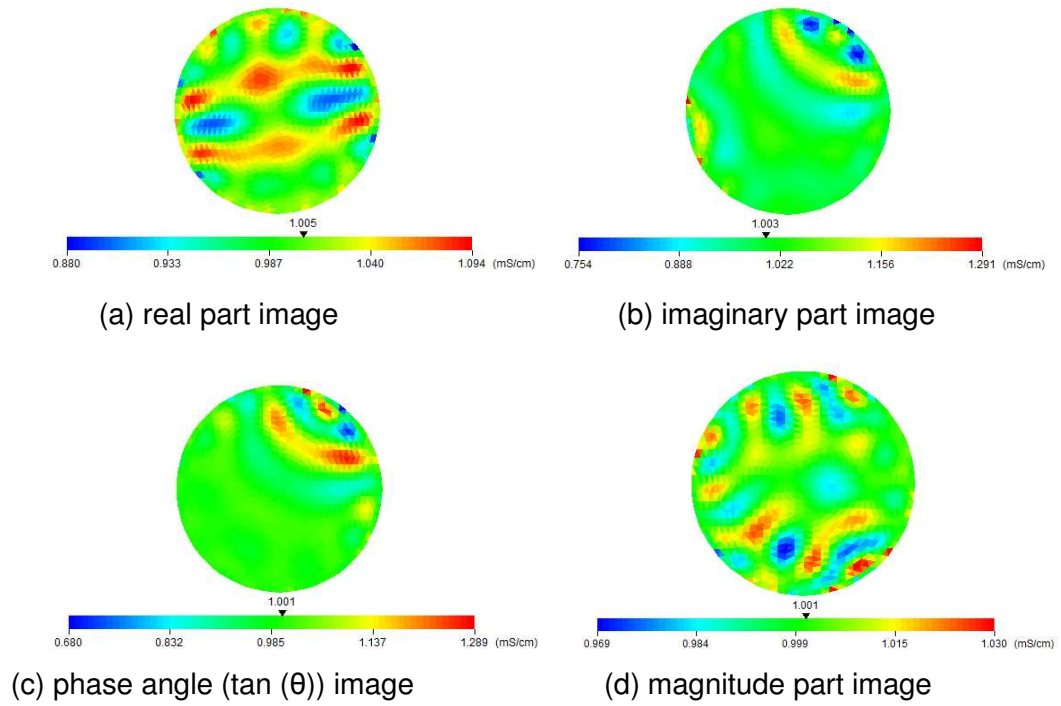


Figure 16: EIT images of silica suspension filled in a chamber (reference is the chamber filled with water in the vessel): (a) real part image, (b) imaginary part image, (c) phase angle ( $\tan(\theta)$ ) image, and (d) magnitude part image

## Figure Captions

Figure 1: Photograph of the vessel with the four-electrode sensor

Figure 2: Photograph of the experimental set-up for EIT measurement

Figure 3: Particle size distribution of SiO<sub>2</sub> nano-particle suspensions

Figure 4: Impedance spectra for silica suspensions ( $\Phi=4.76\%$ ) with different particle size (13.5412 nm, 91.2835 nm, 190.170 nm, 199.790 nm, 384.6220 nm); (a) real and imaginary part vs. frequency; (b) phase angle vs. frequency

Figure 5: Impedance spectra for silica suspensions ( $\Phi=2.38\%$ ) with different particle size (13.5412 nm, 91.2835 nm, 190.170 nm, 199.790 nm, 384.6220 nm); (a) real and imaginary part vs. frequency; (b) phase angle vs. frequency

Figure 6: absolute value of phase angle ( $|\theta|$ ) at 80kHz as function of particle size (d) for silica suspensions ( $\Phi=4.67\%$  and 2.38%)

Figure 7: Schematic of the generation of electrolyte concentration gradient responsible for  $\alpha$  relaxation for a negatively charged particle (E is the applied external electrical field,  $J_{es}^+$  is the tangential electromigration flux of counterions,  $J_{en}^-$  is the normal electromigration flux of the co-ions)

Figure 8: Frequency response of the (a) real; and (b) imaginary part of complex permittivity of silica suspensions ( $\Phi= 4.76\%$ ) for different particle size indicated.

Figure 9: The imaginary part of complex permittivity spectra for silica suspensions with different particle size (a)  $\Phi= 2.38\%$ ; (b)  $\Phi= 0.476\%$ ; (c)  $\Phi= 0.238\%$

Figure 10: The relaxation frequency  $\omega\alpha$  is plotted against  $(a+\kappa-1)$  for silica suspensions (a)  $\Phi= 4.76\%$ ; (b)  $\Phi= 2.38\%$ .

Figure 11: Conductance increment  $\Delta K'$  relative to background electrolyte conductance as function of frequency for silica suspensions (384.5220 nm) with different particle volume fractions ( $\Phi = 4.76\%$ , 2.38%, 0.476%, 0.238%)

Figure 12: The relaxation frequency  $\omega\alpha$  as a function of volume fraction ( $\Phi$ ) for silica suspensions: (a) small particles (13.512 nm, 91.335 nm, 190.170 nm); (b) large particles (199.790 nm, 384.6220 nm).

Figure 13: EIT images of an empty chamber in a vessel (reference is water): (a) real part image, (b) imaginary part image, (c) phase angle ( $\tan(\theta)$ ) image, and (d) magnitude part image

Figure 14: EIT images of chamber (filled with water) in a vessel (reference is the empty chamber fixed in the vessel): (a) real part image, (b) imaginary part image, (c) phase angle ( $\tan(\theta)$ ) image, and (d) magnitude part image

Figure 15: EIT images of silica suspension filled in a chamber (reference is the empty chamber in the vessel): (a) real part image, (b) imaginary part image, (c) phase angle ( $\tan(\theta)$ ) image, and (d) magnitude part image

Figure 16: EIT images of silica suspension filled in a chamber (reference is the chamber filled with water in the vessel): (a) real part image, (b) imaginary part image, (c) phase angle ( $\tan(\theta)$ ) image, and (d) magnitude part image